Fernández-Olivares *et al.*
Cell Communication and Signaling (2025) 23:153
https://doi.org/10.1186/s12964-025-02151-w

Cell Communication and Signaling

RESEARCH

Open Access

Connexin46 in the nucleus of cancer cells: a possible role as transcription modulator

Ainoa Fernández-Olivares[1], Viviana P Orellana[1], Jesús Llanquinao[1,10], Gonzalo Nuñez[1], Pablo Pérez-Moreno[1], Sebastián Contreras-Riquelme[2], Alberto JM Martin[3,4], Fabio Mammano[5], Ivan E Alfaro[1,9], Juan F Calderón[6], Jimmy Stehberg[7], Mauricio A Sáez[8*] and Mauricio A. Retamal[1*]

Abstract

Background Oncogenes drive cancer progression, but few are active exclusively in tumor cells. Connexins (Cxs), traditionally recognized as ion channel proteins, can localize to the nucleus and regulate gene expression, playing key roles in both physiological and pathological processes. Cx46, once thought to be restricted to the eye lens, has been implicated in tumor growth, though its underlying mechanisms remain unclear. This study investigates the nuclear presence of Cx46 in cancer cells and its potential role as a transcriptional modulator.

Methods We employed ChIP-Seq, confocal immunofluorescence, and nuclear protein purification to assess Cx46 localization and DNA interactions. Functional assays were conducted to evaluate its effects on invasion, division, spheroid formation, and mesenchymal marker expression. Single-point mutations and molecular dynamics simulations were used to explore potential Cx46-DNA interactions.

Results Cx46 mRNA upregulation was found in a variety of tumors compared to adjacent healthy tissue. In HeLa cells, which do not express Cx46, its transfection promoted proliferation, invasion and self-renewal capacity, cancer stem cell traits and mesenchymal features. Consistently, in Sk-Mel-2, which naturally express Cx46, reduced Cx46 expression led to a decrease in the similar parameters. In HeLa cells, nuclear Cx46 was detected in two forms, full length 46 kDa and a 30 kDa fragment (GJA3-30 k), ChIP-Seq experiments revealed that Cx46 binds to the DNA at intergenic and promoter regions, leading to the activation of oncogenic pathways. Molecular dynamics simulations suggest that GJA3-30 k dimerizes in a RAD50-like structure, forming stable DNA complexes. Cx46 and in some cases GJA3-30 k were detected in the nuclei of multiple cancer cell lines, including prostate, breast and skin cancers.

Conclusions Our findings reveal a novel nuclear role for Cx46 in cancer, demonstrating its function as a transcriptional regulator and its potential as a therapeutic target.

Keywords Connexin46, Transcription factor, Cancer, IRES

*Correspondence:
Mauricio A Sáez
mauricio.saez.venegas@gmail.com
Mauricio A. Retamal
mretamal@udd.cl
Full list of author information is available at the end of the article

© The Author(s) 2025. **Open Access** This article is licensed under a Creative Commons Attribution-NonCommercial-NoDerivatives 4.0 International License, which permits any non-commercial use, sharing, distribution and reproduction in any medium or format, as long as you give appropriate credit to the original author(s) and the source, provide a link to the Creative Commons licence, and indicate if you modified the licensed material. You do not have permission under this licence to share adapted material derived from this article or parts of it. The images or other third party material in this article are included in the article's Creative Commons licence, unless indicated otherwise in a credit line to the material. If material is not included in the article's Creative Commons licence and your intended use is not permitted by statutory regulation or exceeds the permitted use, you will need to obtain permission directly from the copyright holder. To view a copy of this licence, visit http://creativecommons.org/licenses/by-nc-nd/4.0/.

Introduction

Cancer remains one of the leading causes of mortality worldwide, claiming millions of lives each year [1]. A major challenge in medical research is understanding the molecular mechanisms that drive tumor progression, metastasis, and chemoresistance. Proper gene expression is crucial for maintaining cellular function and homeostasis across tissues and organs. However, cancer disrupts this balance by accumulating harmful genomic alterations in specific regions [2]. Genes that undergo mutations leading to cancer initiation and progression are known as oncogenes [3]. Many oncogenes are also expressed in normal cells, making it difficult to target them therapeutically without affecting healthy tissues, often resulting in undesirable side effects. Therefore, identifying proteins that are either exclusively expressed in cancer cells or have highly restricted expression in normal tissues is critical. Such targets could not only minimize side effects but also play a significant role in tumor progression, offering potential avenues for therapeutic intervention.

Connexin proteins (Cxs) constitute a family of 21 members that assemble into hexameric structures known as hemichannels [4]. These hemichannels facilitate the exchange of molecules, including ions, second messengers, and metabolites, between the cytoplasm and the extracellular space [4]. When two hemichannels from neighboring cells align, they form Gap Junction Channels (GJCs), establishing direct cytosolic communication between adjacent cells [5]. Additionally, Cxs have been reported to exert biological effects independent of their channel-forming function [6–9]. For example, Cx43 has been proposed as a direct transcriptional regulator of N-cadherin in neural crest cells [10]. Moreover, the expression of the C-terminal region of Cx43 in HeLa cells and cardiomyocytes has been linked to its nuclear localization and promotes a significant reduction in cell division rates [11].

Recent studies have also shown that Cx43 is present in the nuclear envelope of cardiomyocytes and other cell types, suggesting its potential role in modulating the transcriptome [12]. Additionally, an alternatively translated isoform of Cx43, GJA1-11 k, has been identified in the nucleus of HEK293FT cells, where it inhibits cell division [13]. Another connexin, Cx26, has been shown to interact with pluripotency-associated transcription factors Nanog and FAK, promoting the self-renewal of triple-negative breast cancer cells [14, 15]. These findings suggest that certain Cxs can localize to the cell nucleus and act as transcriptional regulators in cancer cells. However, both Cx26 and Cx43 are expressed in various cell types, including astrocytes, cardiomyocytes, and hepatocytes [16–18], indicating that they are not exclusively associated with cancer.

In humans, the expression of Cx46 has been found almost exclusively in the eye lens, where it plays a critical role in maintaining lens transparency [19]. However, studies have also detected the presence of Cx46 in breast cancer and glioblastoma cells [20, 21]. Interestingly, its presence in cancer cells has been linked to the acquisition of mesenchymal and cancer stem-like cell (CSC) characteristics [21–25]. These cellular transformations typically involve specific transcriptional regulatory mechanisms. Notably, Cx46 has been found within the cell nucleus of TtT/GF cells, co-localizing with Nopp140, a nucleolar factor involved in rRNA processing [26]. Despite these observations, the role of Cx46 as a transcriptional modulator in cancer cells has not yet been reported. Therefore, this study aims to determine whether Cx46 is found in the cell nucleus of different tumoral cell lines and has a role in gene regulation.

Material and methods

Cell culture and transfections

HeLa, ZR75, MDA-MB-231 cells were cultured in Dulbecco's Modified Eagle Medium (DMEM, Gibco, Thermo Fisher, CA, USA), while LnCap, DU145, PC3, Sk-Mel-2, 397-Mel and Mel-1 cells were maintained in RPMI (Gibco, Thermo Fisher, CA, USA). Both media were supplemented with 10% fetal bovine serum (FBS, Biological Industries, Israel) and 1% Penicillin–streptomycin sulfate (10,000 units/ml penicillin and 100 mg/ml streptomycin sulfate; P/S, Sigma Aldrich, USA). Cells were incubated at 37 °C, 5% CO_2 and 95% humidity.

Cell transfection

HeLa cells were dissociated for subculturing using 0.05% trypsin–EDTA (ThermoFisher Scientific, Rockford, IL. USA) and seeded in 6-well plates. At approximately 60% confluence (24–48 h later), cells were transfected with 1 µg of pRP[Exp]-EGFP/Bsd-CMV > hGJA3 (VectorBuilder, Chicago, USA), containing the human sequence for either wild-type Cx46 or methionine-to-alanine mutants (Supplementary Figure S1). Briefly, 0.5 µg of each plasmid was mixed with Opti-MEM medium (ThermoFisher Scientific, Rockford, IL. USA) and Lipofectamine 2000. The culture medium was replaced with Opti-MEM, and the transfection mixture was added. cells were returned to DMEM supplemented with 10% FBS and incubated at 37 °C in 5% CO_2. Forty-eight hours post-transfection, Cx46 expression was assessed via epifluorescence microscopy. Selection was performed by

adding Blasticidin to the culture medium three times per week for two weeks.

Purification of nuclear and cytoplasmic proteins

The purification was carried out following a previous protocol [27] with minor modifications. Briefly, one 100 mm plate per condition was seeded 48 h before the assay. Then, the cells were washed with phosphate buffered saline (PBS). Using a cell scraper, the cells were collected and centrifuged at 500×g for 5 min at 4ºC. The resulting pellet was used for the extraction of cytoplasmic and nuclear proteins using the NE-PER Nuclear and Cytoplasmic Extraction Reagents kit, following the manufacturer's protocol (ThermoFisher Scientific, Rockford, IL. USA).

Western blot

Cells at 60–80% confluence were scraped using a robber policeman in ice-cold PBS supplemented with protease and phosphatase inhibitors (Cell Signaling, MA, USA) and then sonicated on ice. Protein concentration in the cell lysate was measured using a Qubit Protein Assay Kit (ThermoFisher Scientific, Rockford, IL. USA) and quantified with a Qubit 3.0 Fluorometer (ThermoFisher Scientific, Rockford, IL. USA). A 4×sample buffer was added to each cell homogenate, mixed and heated at 95 °C for 3 min. Forty micrograms of protein were loaded onto a 10% NuPAGE™ gel (ThermoFisher Scientific, Rockford, IL. USA) and subsequently transferred to a PVDF membrane using an iBlot Gel Transfer Device (ThermoFisher Scientific, Rockford, IL. USA). The PVDF membrane was blocked with a solution composed of 5% milk in Tris Buffer and 0.05% Tween 20 (TTBS) for 1 h at room temperature (RT) under agitation. The membrane was then incubated overnight at 4 °C with primary antibodies: anti-Cx46 antibody (Santa Cruz Biotechnology, 1:500), anti-GAPDH (Santa Cruz Biotechnology, 1:1000) and anti-Lamin B1 (Santa Cruz Biotechnology, 1:1000). The next day, membranes were washed three times with TTBS and incubated with a horseradish peroxidase (HRP)-conjugated secondary antibody (Abcam, Cambridge, UK) for 1 h at RT, followed by three additional washes with TTBS. Protein detection was carried out using the SuperSignal West Atto chemiluminescent substrate (ThermoFisher Scientific, Rockford, IL. USA) and visualized with the iBright 1500 Chemiluminescence Scanner system (ThermoFisher Scientific, Rockford, IL. USA).

Indirect immunofluorescence

Cells were seeded on glass coverslips and allowed to reach 80% confluence before processing. They were then washed twice with PBS and fixed with 4% paraformaldehyde for 20 min. Permeabilization was performed with PBS-0.1% Triton for 10 min. After washing with PBS, blocking was performed with 4% bovine serum albumin (BSA, Winkler, Santiago, Chile) and 0.3 M glycine in PBS with 0.1% Tween 20 (PBS-T) for 30 min. The coverslips were washed with PBS-T and incubated overnight at 4 °C with primary antibodies: anti-Connexin46 (SC-365394, Santa Cruz Biotechnology) and anti-Histone H3K9 (MA5-11,195, Invitrogen), both diluted in 1% BSA. The following day, coverslips were washed three times with PBS-T and incubated for 2 h at RT with secondary antibodies: Alexa Fluor 355 goat anti mouse (ThermoFisher Scientific, Rockford, IL. USA) and Alexa 555 goat anti-Rabbit (ThermoFisher Scientific, Rockford, IL. USA) 1:400. Finally, the coverslips were washed 3 times with PBS-T and mounted with Fluoromount-G (ThermoFisher Scientific, Rockford, IL. USA) on glass slides.

Colony forming unit assay

Cells were trypsinized and counted to seed a total of 300 cells in a 35 mm plate. After 12 days, the cell colonies were fixed with 4% paraformaldehyde and stained with 10% (w/v) crystal violet. A cluster of more than 100 cells was considered a colony. Colonies were manually counted and photographs were taken of the entire well.

Spheroid formation

A total of 1×10^5 cells were seeded in 200 µl of supplemented medium in 96-well plates pre-coated with 50 µL of 1.5% agarose to prevent adherence and promote spheroid formation. After four days, spheroids were imaged using a 4×objective on a Nikon epifluorescence microscope (Ti Eclipse) and maintained in culture for up to 14 days, with half the volume of the media (100 µL) changed every three days. The spheroid area was quantified using ImageJ to assess size differences.

Matrigel invasion assay

The transwell invasion assay was performed by adding an extracellular matrix layer on top of a porous membrane, allowing only cells with invasive properties, such as tumor cells, to undergo chemotaxis and migrate through the membrane [28]. A total of 60 µL of Matrigel was added to 6.5 mm diameter polycarbonate transwells with an 8 µm pore size and incubated for 2 h at 37 °C with 5% CO_2 and 95% humidity. Subsequently, 100,000 HeLa-P or HeLaCx46 cells, resuspended in 100 µL of DMEM with 2% FBS, were added to the upper chamber, while the lower chamber contained DMEM supplemented with 20% FBS to create a chemotactic gradient. After 72 h of incubation, non-migrated cells were removed using a

cotton swab. The insert was then fixed with 4% PFA and stained with DAPI for quantification of cell nuclei [28]. Invasive cells were counted in 5 random fields of view (FOV = 336 mm^2 total) at 20X magnification using a Nikon Eclipse Ti epifluorescence microscope.

qPCR

Experiments were conducted as described elsewhere [29]. Briefly, total RNA was extracted from cells using the EZNA Total RNA Kit I (Omega Bio-Tek, Norcross, GA, USA). RNA concentration was measured with a Cytation 5 imaging reader (Biotek Instruments Inc., Winooski, VT, USA). cDNA was synthesized from total RNA using the AffinityScript QPCR cDNA Synthesis Kit (Agilent Technologies, Bastrop, TX, USA) following the manufacturer's instructions. Quantitative real-time PCR was performed on an AriaMX Real-Time PCR System (Agilent Technologies, Bastrop, TX, USA) using SYBR Green PCR Master Mix (Thermo Fisher Scientific, Waltham, MA, USA). The PCR protocol consisted of an initial denaturation at 95 °C for 5 min, followed by 40 cycles of 95 °C for 10 s and 60 °C for 45 s, with a final step at 95 °C for 15 s, 60 °C for 1 min, and 95 °C for 15 s. Reactions were conducted in triplicate, and relative mRNA abundance was calculated using the $2^{\wedge\Delta\Delta Ct}$ method, normalized to GAPDH.

GJA3 mRNA expression across different tumor types

The results presented here are based on data generated by The Cancer Genome Atlas (TCGA) research network "https://www.cancer.gov/tcga". We obtained all gene expression profiles available from the TCGA-ARCHS4 data repository [30]. For each tumor type, we compared gene expression between tumor and surrounding healthy tissue for all 22 tumor types with available data using DESeq2 [31]. We then analyzed whether GJA3 was differentially expressed in tumors or healthy samples. The mean and absolute standard deviation of these data was computed. Additionally, a Mann–Whitney U-test was performed to determine if GJA3 expression profiles differ between tumor and normal tissue. This test assesses the statistical confidence that the DESeq2-normalized expression of a given gene is consistently higher in one condition than in the other.

Chromatin Immunoprecipitation (ChIP)

For a detailed protocol on the Cx46-DNA interaction ChIP-Sec method please refer to [32]. Briefly, nuclear extracts were prepared from HeLa-P and HeLa Cx46WT. A total of 2×10^7 cells were washed with PBS and crosslinked with 1% Formaldehyde under gentle agitation at RT. After 10 min, glycine was added at a final concentration of 0.125 M and incubated for an additional 10 min under agitation. Cells were then washed 3 times with PBS and collected using a cell scraper. The pellet was resuspended in 5 volumes of lysis buffer (50 mM HEPES pH: 7.8, 3 mM $MgCl_2$, 20 mM KCl, 0.1% NP-40, 2 mM phenylmethylsulfonyl fluoride (PMSF), 2 µg/ml aprotinin, 2 µg/mL leupeptin and 1 µM pepstatin). Samples were then incubated for 10 min on ice. Purified nuclei were obtained using a glass Dounce homogenizer and verified by Trypan Blue staining. Nuclei were centrifuged and resuspended in Sonication Buffer (50 mM HEPES pH: 7.8, 140 mM NaCl, 1 mM EDTA, 1% Triton X-100, 0.1% Sodium Deoxycholate, 1% Sodium Dodecyl Sulfate, 2 mM PMSF, 2 µg/ml aprotinin, 2 µg/mL leupeptin and 1 µM pepstatin). Samples were transferred to Bioruptor sonication tubes and sonicated for 50 min at 30 s intervals on a Bioruptor Pico sonication device. The degree of chromatin fragmentation was verified on a 1% agarose gel. Decrosslinking was performed in a thermocycler at 95 °C for 25 min, followed by treatment with 2 µg/mL RNase A at 37 °C for 15 min and 50 µg/mL proteinase K at 58 °C for 15 min. DNA was quantified using the Qubit dsDNA BR Assay Kit on a Qubit Fluorometer according to the manufacturer's instructions.

To perform the immunoprecipitation, 200 ng of DNA were set aside as input, while 400 ng of DNA was used for the ChIP. Pre-clearance was carried out using mouse IgG (12–371, Merck Millipore) or rabbit IgG (12–370, Merck Millipore) bound to protein G or protein A, respectively, for 2 h at 4 °C. Subsequently, the samples were washed twice with washing buffer (100 mM Tris–HCl pH: 8.0, 500 mM LiCl, 1%NP-40 and 1% sodium deoxycholate), centrifuged at 4000 rpm at 4 °C and the supernatant was transferred to a new tube. Dynabeads M-280 sheep anti mouse IgG with 4 µg of anti-Connexin46 (SC-365394, Santa Cruz Biotechnology), 4 µg of mouse IgG, Dynabeads M-280 Sheep anti Rabbit IgG with anti H3K27AC or IgG of rabbit were added. Samples were incubated overnight at 4 °C after which, Dynabeads were collected using a magnet. DNA was recovered by adding 100 µL of elution buffer (50 mM NaHCO3, 1% SDS, 2 mM PMSF, 2 µg/mL aprotinin, 2 µg/mL leupeptin and 1 µM pepstatin). Samples were vortexed and incubated at 65 °C for 15 min. Then, 4 µL of 5 M NaCl and 1 µg of RNase A were added, and the samples were incubated overnight at 65 °C. Proteinase K 50 µg/mL was added, and samples were incubated for 2 h at 50 °C. DNA was extracted using 200 µL of TE pH: 7.8 and one volume of Phenol:Chloroform:Isoamyl alcohol, centrifuged at 15,000 × g at 4 °C for 10 min and the aqueous phase was transferred to a new tube. A second extraction was performed using 1 volume of Chloroform:Isoamyl Alcohol (24:1), followed by ethanol precipitation overnight at −20 °C, with 2.5 volumes of absolute ethanol, 0.1 volumes

of sodium acetate 3 M pH: 7.0 and 20 µg of glycogen. The DNA was centrifuged for 25 min at 12,500 × g at 4 °C, and the DNA pellet was washed with 70% ethanol, allowed to dry, and resuspended in TE buffer before quantification and agarose gel verification.

Generation of DNA libraries

DNA libraries were prepared using the Microplex Library Preparation kit V2 according to the manufacturer's instructions with 10 ng of DNA from both immunoprecipitated samples and inputs as starting material. Adapter ligation was performed using Illumina-compatible adapters and indices. NGS Illumina platform was used for multiple sequencing. Library amplification was conducted with 10 PCR cycles for inputs and 13 cycles for immunoprecipitated samples. Libraries were purified using AMPure XP magnetic beads at 0.7 times the volume of the samples. The beads were separated using a magnet, washed with 70% ethanol twice and eluted with 20 uL of Tris pH: 8.0. Final DNA quantification was performed using the Qubit dsDNA HS Assay Kit on a Qubit Fluorometer and size was assessed via 1% agarose gel electrophoresis.

DNA sequencing

Library quality was analyzed using an Bioanalyzer Agilent 2100 and sequencing was performed on an Illumina HiSeq system with 150-cycle pair-end mode reads. ChIP-seq data were validated by qPCR for four target genes, using promoter-specific primers designed with Primer3 program [33]. Cx46 enrichment was determined using a set of 47,656 transcription start sites (TSS), displaying only those reads located upstream and downstream of a 5 kb window.

RNA extraction

Total RNA from HeLa cells expressing pCAG-Connexin46 or untransfected controls were extracted using RNA-Solv® Reagent. RNA-Solv (1 ml) was added to the 3.5 cm culture plates at 80% confluence, pipetted to help with lysis, and then transferred to a tube where 200 µL of chloroform was added and vortexed for 15 s. The samples were incubated on ice for 10 min and centrifuged at 12,000 × g for 15 min. The aqueous phase was transferred to a new tube and 500 µL isopropyl alcohol was added, incubated again for 10 min and centrifuged at 12,000 × g for 10 min. The supernatant was discarded and the pellet was washed with 80% ethanol. Finally, the pellet was centrifuged at 7500 × g for 5 min and left to dry for 5 min. The pellet was resuspended in nuclease-free water and quantified on a Nanoquant Plate in a TECAN infinite F200 equipment. The quantified samples were stored at −80 °C.

RNA sequencing

Total RNA extraction was digested with DNase I to avoid contamination with genomic DNA. RNA concentration was then measured using Quant-iT™ RiboGreen® RNA Assay Kit and its integrity was determined with a Agilent Bioanalyzer 2100. RNA libraries were prepared using the IlluminaTruSeqTM RNA Kit (High Throughput Protocol) following the manufacturer's protocol. Ribosomal RNA (28S, 18S, 5.8S, and 5S rRNA) was depleted using the Ribo-Zero rRNA removal kit from an initial 500 ng of total RNA from each sample. The resulting RNA was cleaved with divalent cations at 95 °C, and the fragmented RNA was reverse-transcribed into cDNA to produce single-stranded DNA copies. After synthesis of the second cDNA strand, the ends were repaired, the 3' ends adenylated, the cDNAs were ligated with universal adapters, and amplified by PCR to produce the final sequencing library. After validation of the library with the DNA 1000 ChIP using the Agilent Technologies 2100 bioanalyzer, the samples were pooled at equal concentrations and sequenced using an Illumina HiSeq with 100-cycle paired-end reads.

Validation of transcriptome sequencing results

To validate transcriptome data, 4 genes related to cancer progression were selected. Primers were chosen from the Primer Bank database. cDNA synthesis was carried out using the high-capacity cDNA reverse transcription kit (Applied Bioscience) following the manufacturer's instructions. The qPCR was performed using QuantStudio2 with Brilliant II SYBR green qPCR Master Mix (Agilent), and included 95ºC for 10 min, 40 cycles of 95 °C for 15 s, 60ºC for 30 s and 72ºC for 60 s. The GAPDH gene was used as an endogenous reference gene and the relative expression (shown as fold change) of HeLa-Cx46 samples over HeLa cells, was calculated for each gene using the $2^{-\Delta\Delta Ct}$ method.

ChIP-seq and RNA-seq analysis

The adapter sequences and low-quality reads were removed using Trim Galore software and the sequencing reads were aligned to the human reference genome (GRCh38) using Bowtie2. Peak calling was performed using MACS3 ($q \leq 0.01$). Peak distribution was analyzed with HOMER [34] and ChIPSeeker [35], while motif enrichment was conducted with MEME [36].

Regulatory network analysis

Gene regulatory networks (GRNs) for both control and GJA3 conditions were developed following methodologies from previous studies [37, 38]. Outgoing edges of expressed TFs were kept, while those arising from non-expressed TFs were removed from the union of high

confidence general GRNs deposited in TRRUST [39], RegNetwork [40] and DoRothEA [41, 42]. As regulatory events guided by GJA3 are not annotated in these databases, we identified overlapping peaks of GJC3 with promoter regions defined by the Ensembl consortia [43], assigning regulation of GJA3 to the closest gene in the human genome (version GRCh38). Master Regulators (MRs) were identified for the control and GJA3 conditions. For genes defined as differentially expressed, their first and second upstream neighbors in both networks were selected [37]. Then, nodes with the highest edge density were identified [44], via iterative steps deleting nodes with lower out-degree until the deletion of a node in the subnetwork resulted in an unconnected network (supplementary script getRM.py), with remaining TFs being categorized as candidates to be MRs. Finally, fulfillment of the definition of MR [44] for predicted candidates was determined by observing whether a candidate regulated other MF candidates, it was regulated by other candidates and showed physical interactions between them [45].

Modeling and molecular dynamics simulation

A model of the Cx46 hexamer and the DNA-binding 30 kDa dimmer peptide (GJA3-30 k) was constructed using the AlphaFold 3 server [46]. Five models for each of the five DNA sequences experimentally determined as target sequences for Cx46 were simulated. The resulting structures were clustered, and the center of the most populated cluster was selected for molecular dynamics (MD) simulations. The MD simulations were performed using GROMACS [47]. In brief, the system was solvated in a water box with 0.15 M NaCl using CHARMM-GUI [48], and an energy minimization and equilibration was followed by a 500 ns production step with the Charmm36 forcefield. Post-simulation clustering was done using MDAnalysis [49] and the center of the most populated cluster was processed using the Dali Server [50] to identify proteins with similar structural features, particularly those with DNA-binding properties.

Results

The expression levels of Cx46 mRNA exhibit a significant increase in human neoplastic tissues

As previously reported, Cx46 has been detected in breast cancer and glioblastoma [20, 21]. However, its expression in other cancer types remains undocumented. To address this gap, Cx46 mRNA levels were analyzed across various human cancer types using data from the Cancer Genome Atlas (TCGA) database [51]. Our analysis revealed a significant upregulation of Cx46 mRNA levels in multiple cancer types, including Breast Invasive Carcinoma (BRCA), Cholangiocarcinoma (CCAS), Colon Adenocarcinoma (COAD), Head and Neck Squamous Cell Carcinoma (HNSC), Lung Adenocarcinoma (LUAD), Prostate Adenocarcinoma (PRAD), and Thymoma (THYM), compared to their respective adjacent healthy tissues (Fig. 1). These findings suggest that Cx46 expression in cancer cells is a widespread phenomenon, highlighting the need for further investigation into its molecular mechanisms and role in cancer progression.

The presence of Cx46 enhances proliferation, invasion and self-renewal capacity in HeLa cells

HeLa cells, which derive from cervical cancer, are extensively used in Cx-related research, mainly because these cells typically lack functional GJCs or hemichannels due to minimal or absent Cx expression [52]. Consequently, transfecting HeLa cells with Cx-encoding cDNA has served as a valuable model for studying Cx properties. Upon transfection with Cx46 cDNA, HeLa cells (HeLa-Cx46) exhibited two protein bands (~30 and ~46 kDa) that were absent in non-transfected cells (HeLa-WT) (Fig. 2a). Under normal conditions, HeLa-WT cells grow in patches, with an epithelial-like phenotype (Fig. 2b). In contrast, HeLa-Cx46 cells at the periphery of cell patches exhibit an elongated morphology, often distant from neighboring cells (Fig. 2b), resembling a mesenchymal-like phenotype [53]. Moreover, HeLa-Cx46 cells exhibited a significantly higher proliferation rate compared to HeLa-WT cells (Fig. 2c and Supplementary Table S1). To further confirm this mesenchymal transformation, invasion assays were conducted, which demonstrated that HeLa-Cx46 cells had a significantly higher invasive capacity —~37 times greater—than HeLa-WT cells (Fig. 2d and Supplementary Table S1). Consistently, Cx46-expressing cells displayed elevated mRNA levels of key mesenchymal markers, including Slug, N-Cadherin, Snail, and Vimentin, compared to non-expressing cells (Fig. 2e and Supplementary Table S1). Then we compared the CSC-characteristics in Hela- WT and -Cx46. First we studied the ability of HeLa cells to form colonies, using a colony-forming unit (CFU) assay [54]. HeLa cells with or without Cx46 expression were seeded on a non-adherent surface and allowed to grow for 14 days. Remarkably, HeLa-Cx46 cells formed ~3.8 times more colonies than HeLa-WT cells (Fig. 2f and Supplementary Table S1). Since spheroid formation is commonly used to study the CSC phenotype [55], we explored this capacity on Hela cells. We observed that Cx46-expressing cells successfully formed spheroids, which, although not perfectly round, were compact and displayed a dense core, consistent with previous reports of spheroids formed by other cancer cells [56]. In contrast, non-expressing cells failed to form spheroids and instead remained as a monolayer at the bottom of the non-adherent surface (Fig. 2g).

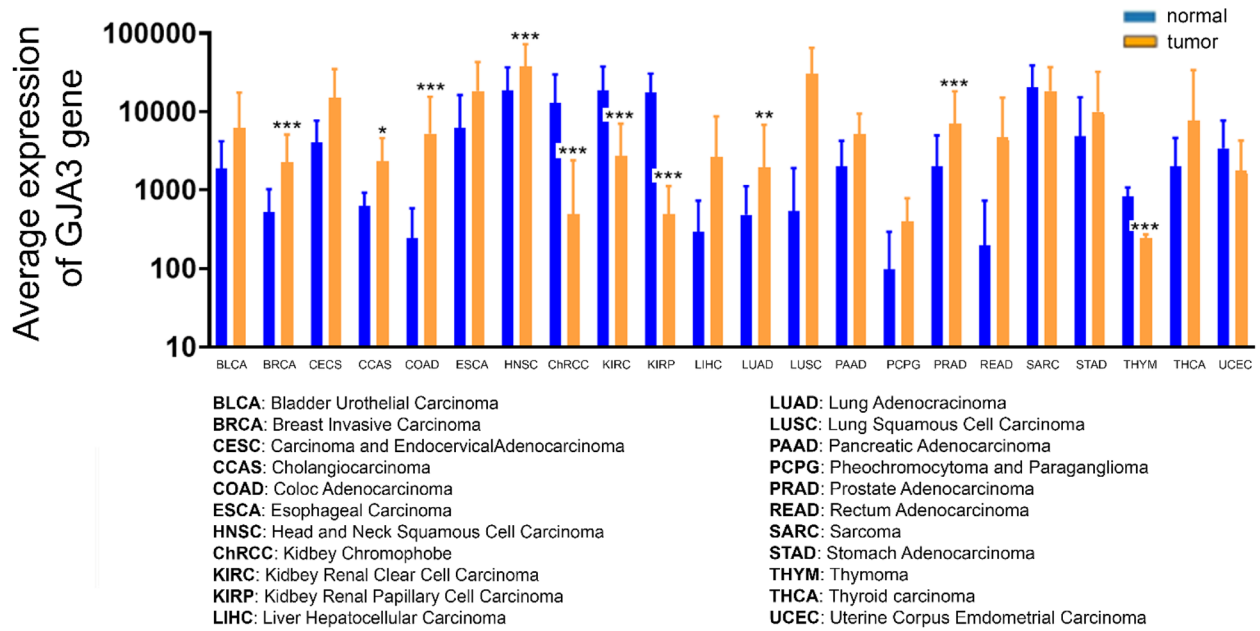

Fig. 1 Gene expression levels of Cx46 in various cancer types. Gene expression data was obtained from the publicly available TCGA repository. This analysis compares the average expression of the GJA3 gene (encoding Cx46) in different tumor types (yellow bars) with the expression in corresponding healthy tissues (blue bars). Each bar represents the mean ± SD. Statistical significance was assessed using the Mann–Whitney U test. These findings provide valuable insights into the dysregulation of Cx46 gene expression across various cancer types, suggesting a potential for Cx46 in the pathogenesis of these malignancies

Since HeLa cells exhibit minimal Cx expression, they are suitable for gain-of-function experiments involving Cx46 overexpression. However, it is important to determine whether the observed effects are specific to HeLa cells or extend to other cancer types. To address this, we performed loss-of-function experiments using a human melanoma cell line (Sk-Mel-2), which naturally express Cx46. We developed a Sk-Mel-2 cell line with a reduced Cx46 expression (Sk-low) using shRNA targeting Cx46 mRNA. As a control (Sk-ctrl), we used a non-targeting shRNA scramble sequence. Post-transfection, Cx46 levels in Sk-ctrl cells remained similar to Sk-wild type (Sk-WT), whereas Sk-low cells showed a ~ 70% reduction in Cx46 expression (Supplementary Figure S2a). We investigated the influence of Cx46 on Sk-Mel-2 cell proliferation, migration, and invasion. In proliferation experiments, Sk-ctrl and Sk-low cells exhibited similar cell numbers until day four. However, by day five, Sk-ctrl cells showed a significant increase in cell number compared to Sk-low cells (Supplementary Figure S2b and Table S2), suggesting that Cx46 promotes cell division or reduces cell death. To further confirm the effect of Cx46 on proliferation, we performed Ki-67 immunofluorescence staining, which revealed ~ 100% Ki-67-positive nuclei in Sk-ctrl cells compared to ~ 40% in Sk-low cells on day five. This supports the role of Cx46 in promoting proliferation rather than inhibiting cell death (Supplementary Figure S2c). Then, we assessed invasion and migration experiments in Sk-Mel-2 cells. After 24 h, the number of SK-ctrl that crossed the Matrigel was higher than SK-low (Supplementary Figure S2d and Table S2). Migration was assessed using a wound healing assay at 4, 8, 24 and 48 h after creating a scratch. At 4 and 8 h, both SK-ctrl and SK-low cells exhibited a similar closure of the cell-free area. However, at 24 h (~ 1.8 times) and at 48 h (~ 1.9 times), the closure in SK-ctrl cells was significantly greater than in SK-low cells (Supplementary Figure S2e and Table S2). To evaluate the presence of CSC properties, we assessed spheroid formation, a key indicator of the CSC phenotype [57, 58]. SK-ctrl cells formed large spheroids after 14 days of culture on a non-adherent surface. In contrast, SK-low cells formed spheroids ~ 65% smaller in size (Supplementary Figure S2f and Table S2). These results indicate a correlation between Cx46 expression and an enhanced CSC phenotype. Our findings in both HeLa and Sk-Mel-2 cells align with our previous research on MCF-7 cells, a human breast cancer cell line, where Cx46 expression was associated with increased epithelial-to-mesenchymal transition [24] and CSC-like properties [24]. Both traits have been strongly linked to distinct gene regulatory programs [59], suggesting that Cx46 may function

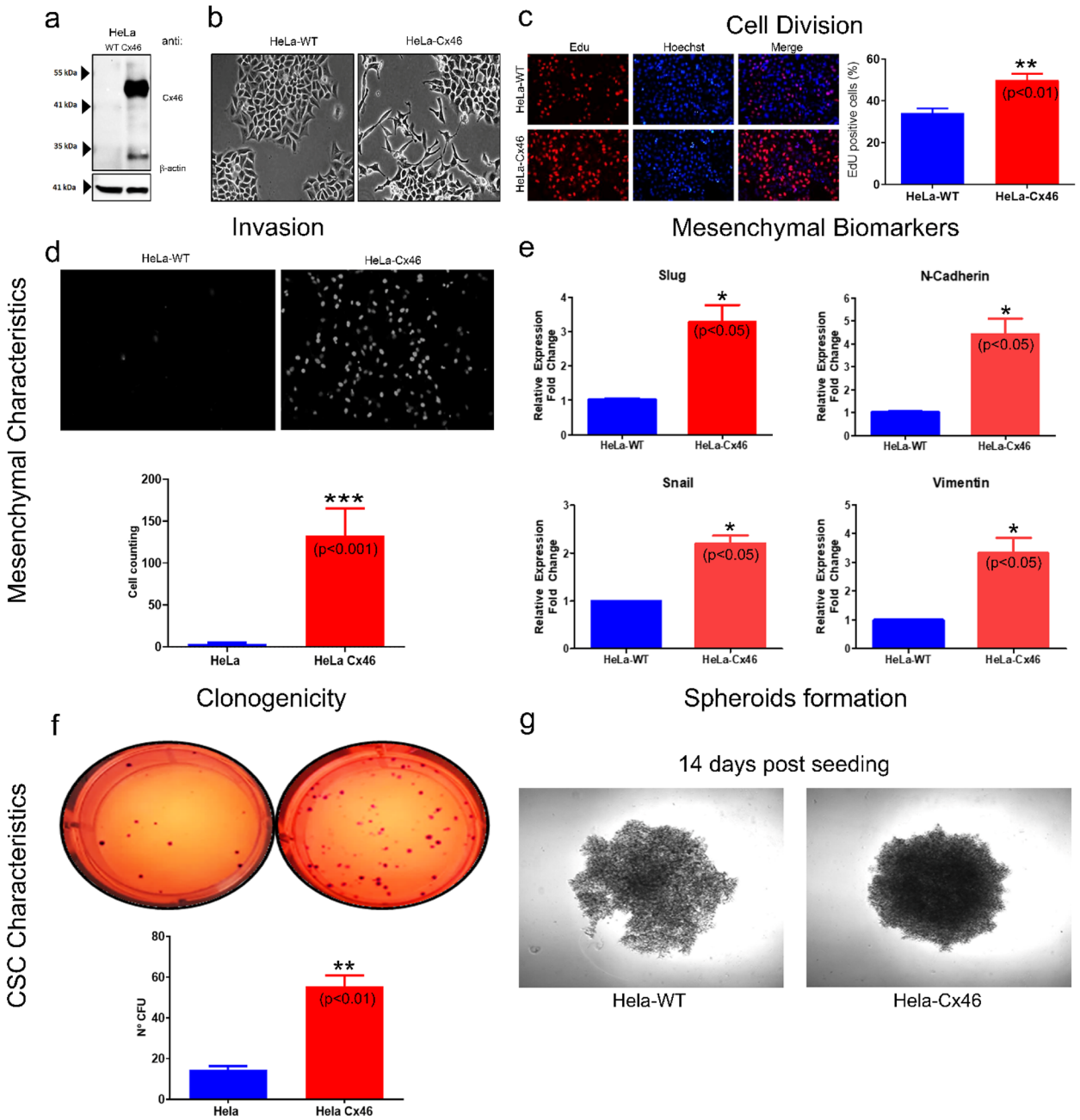

Fig. 2 Effects of Cx46 expression on the proliferation, invasion, and stemness of HeLa cells. **a** Representative Western blot of wild-type (WT) and Cx46-expressing HeLa cells. A Cx46-specific antibody targeting the C-terminal region of the protein was used, with β-actin as a loading control. Cx46 and actin bands were visualized using an HRP-conjugated secondary antibody. **b** Phase-contrast microscopy of HeLa WT and HeLa-Cx46 cells, revealing morphological differences. **c** Proliferation assay was performed by incorporating EdU (a thymidine analog) into dividing cells for 4 h, followed by detection using an epifluorescence microscope (red). Hoechst staining (blue) was used to determine the total number of cells after fixation. The graph presents the mean ± SE of EdU-positive cells relative to Hoechst-stained cells. Statistical analysis was performed using the Mann–Whitney U test. **d** Invasion assay was conducted using a transwell system, assessing the ability of cells to traverse an extracellular matrix over 72 h. The upper panel shows representative images of invaded cells with DAPI-stained nuclei. The lower panel quantifies the number of invaded cells (mean ± SE, from three independent experiments). Statistical analysis was conducted using the Mann–Whitney U test. **e** Mesenchymal marker expression was analyzed by qPCR. Graphs display the quantification of three independent experiments. **F**-**G** Stemness was assessed using a colony-forming unit (CFU) assay and a spheroid formation assay. For CFU, 35 mm dishes were seeded with 50 cells and after 14 days, the colonies were stained with crystal violet. (mean ± SE, from three independent experiments). Statistical analysis was conducted using the Mann–Whitney U test. **g** For the spheroid formation assay, cells were seeded cells in a non-adherent culture system for 14 days and images were taken using a Nikon Eclipse-Ti ($n = 3$)

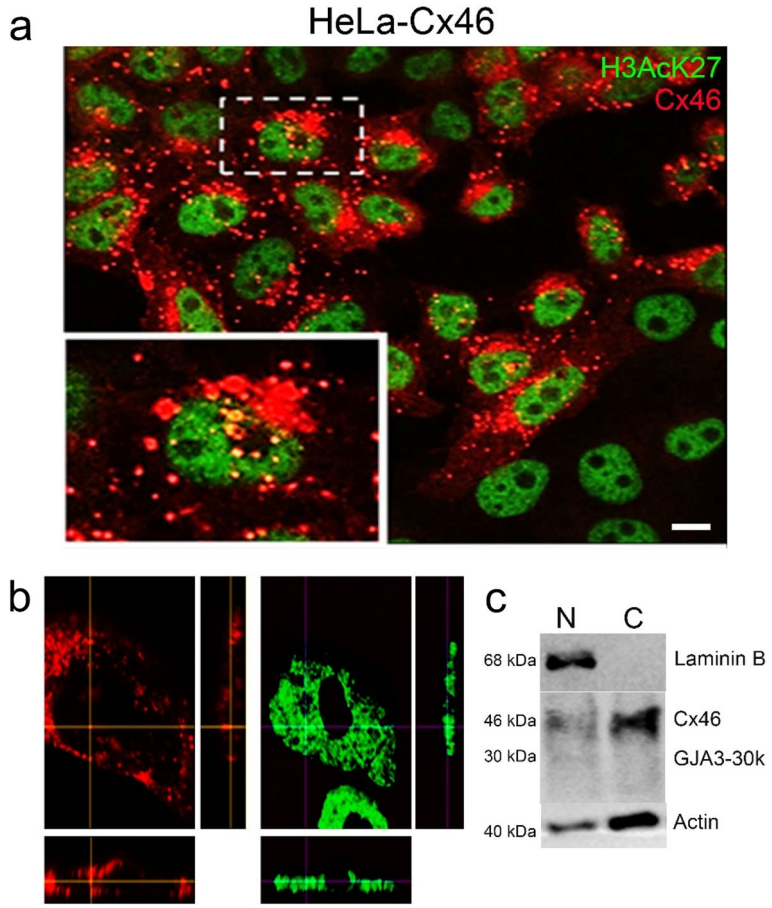

Fig. 3 Cx46 exhibits nuclear localization in HeLa cells. **a** Representative confocal images captured using a 60× oil objective. HeLa-Cx46 cells were fixed and stained with an anti-Cx46 antibody (red) and an anti-H3acK27 antibody (green). The zoomed-in inset in the lower left corner highlights a specific region of the field, marked by a white segmented square. Co-localization of the red and green appears as yellow, indicating the presence of Cx46 in the nucleus. Scale bar = 10 mm (**b**) Orthogonal view: Orthogonal projections generated from different planes provide a three-dimensional perspective of Cx46's subcellular localization. These views confirm its presence in the nucleus. **c** Western blot analysis of cellular fractions: Cytoplasmic (C) and nuclear (N) protein samples were analyzed by Western blot. Cx46 was detected in both cytoplasmic and nuclear samples, appearing as two major bands (~30 and 46 kDa). An antibody against Laminin B (nuclear protein) was used as a control, which recognizes nuclear samples and not cytoplasmic samples (~68 kDa)

as a master regulator of genes associated with cancer aggressiveness.

Cx46 exhibits localization within the nucleus of HeLa cell transfectants

To investigate the hypothesis that Cx46 functions as a modulator of gene expression, we conducted subcellular localization studies using confocal microscopy. Our observations revealed that while Cx46 was predominantly localized in the cytoplasm of HeLa cells, it also exhibited a nuclear localization. Within the nucleus, Cx46 formed discrete puncta that partially co-localized with the transcription-prone histone mark H3K27Ac (Fig. 3a) and H3K9Ac (Supplementary Figure S3). To further validate these findings, we performed 3D reconstructions of the cell nucleus using series of confocal z-stacks images. These reconstructions confirmed the presence of Cx46 in small foci within the cell nucleus (Fig. 3b). To provide additional confirmation, we isolated cell nuclei and quantified Cx46 protein levels through Western blot analysis. Nuclear samples (N) exhibited two immunoreactive bands corresponding to approximately 30 and 46 kDa (Fig. 3c). To assess sample purity, we utilized an antibody specific to Laminin B, a nuclear protein [60]. The Laminin B signal was exclusively detected in the nuclear samples and absent in the cytoplasmic samples. Actin was present in the nuclear sample [61], but showed greater expression in the cytoplasm. Collectively, these results confirm the presence of Cx46 in the nucleus, suggesting potential

interactions with chromatin, particularly in transcriptionally active regions.

Cx46 binds to DNA, primarily in promoter regions

Given the nuclear localization of Cx46 in the nucleus of HeLa cells, we next sought to determine whether it interacts directly with DNA. To address this, we performed chromatin immunoprecipitation followed by DNA sequencing (ChIP-seq) using an anti-Cx46 antibody targeting the C-terminal (CT) region. This assay confirmed the interaction of Cx46 with DNA, as indicated by the presence of immunoprecipitated DNA fragments. High-throughput sequencing revealed that 47.29% of the precipitated fragments corresponded to promoter regions (Fig. 4a), with a strong enrichment near transcription start sites (TSSs) (Fig. 4b). Further analysis identified specific binding sequences, some of which overlapped with transcription factor (TF) motifs, including FOXJ3, ZN770, and ZN263, while others appeared unique to Cx46 (Fig. 4c). The analysis of TSS regions bound by Cx46 unveiled two distinct clusters of genes. The first cluster encompassed genes involved in Rho GTPase signaling, endoplasmic reticulum (ER) processes, VEGFR2 receptor pathways, Hox-mediated gene activation, and histone deacetylase activity. The second cluster primarily contained genes associated with cell cycle regulation (Fig. 4d). Comparative RNA-seq analysis of HeLa cells with and without Cx46 expression identified 77 differentially regulated mRNAs (Fig. 4e). Notably, IFITM1, TFF1 and FAM83a, which have been strongly associated with cancer aggressiveness and poor prognosis [62–65] were significantly upregulated. To validate our RNA-seq results, we performed RT-qPCR for these three genes and for Cx46. The overexpression of Cx46 was associated with a substantial increase (~10,000 times) in its mRNA level, while IFITM1, TFF1, and FAM83a mRNA levels were elevated 9.9, 2.5, and 2.2 times, respectively (Supplementary Figure S4). These findings suggest that Cx46 binding to promoter regions influences gene expression patterns linked to cancer progression, particularly in aggressive forms of cancer.

Cx46 functions as both an enhancer and a repressor of genes linked to cancer aggressiveness

To examine the correlation between Cx46 promoter binding, gene expression changes, and phenotypic alterations, we integrated ChIP-seq and RNA-seq datasets. We identified 22 genes that exhibited both differential expression and significant Cx46 enrichment in their promoter regions (Fig. 5a). Interestingly, some differentially expressed genes lacked direct Cx46 interaction, suggesting the involvement of an intermediate factor (Fig. 5a). To gain further insights into the regulatory relationship between Cx46 and the expression of these genes, we performed a gene regulatory network analysis. This analysis involved integrating experimental data with information from databases, enabling us to elucidate connections between genes. Notably, Gene regulatory network analysis revealed a link between Cx46 and TFF1/IFITM2, which are regulated by c-Jun—a TF whose promoter region displays an enrichment of Cx46 (Fig. 5b). This finding strengthens the association between Cx46 and the regulation of these specific genes within the broader gene regulatory network.

Alternative translation produces the 30 kDa GJA3-30 k isoform, potentially involved in DNA interactions

Recent studies have confirmed the presence of Cx43 hemichannels at the nuclear envelop, suggesting that Cx43 hemichannel C-terminal regions interact with TFs to modulate gene transcription [12]. Using AlphaFold-generated models of Cx46, we confirmed a typical hemichannel structure (Fig. 6a). Unexpectedly, none of the models suggested direct DNA binding, suggesting that intact Cx46 hemichannels are unlikely to directly bind to DNA (Fig. 6a). Given that connexins Cx32 and Cx43 have alternatively translated isoforms [66–69], some of which localize to the nucleus [13] and modulate cancer cell behavior [69], we hypothesized that

(See figure on next page.)

Fig. 4 Analysis of the DNA binding properties of Cx46. **a** Distribution of Cx46 Enrichment Peaks. This panel shows the distribution of Cx46 enrichment peaks throughout the genome, indicating the percentage of enrichment peaks in across genomic regions. **b** Heat Map of Cx46 enrichment: A heat map representation shows Cx46 binding around the transcription start site (TSS) within a ± 5 kbp region. The left side represents the unenriched chromatin IgG control, while the right-side displays where Cx46 is bound to DNA, highlighting its preferential binding sites. **c** Sequence analysis: Analysis of the DNA sequences that most commonly bind to Cx46. The left side displays sequences specific to Cx46 binding, whereas the right side shows sequences that interact with both Cx46 and other transcription factors. **d** The gene ontology of the genes associated with the enrichment cluster derived from the heat map is presented. The ontology of cluster 1 is shown above, and the ontology of genes derived from cluster 2 is shown below. This analysis provides insights into the functional categories and biological processes associated with those genes that show Cx46 binding. **e** Fold changes in gene expression: A comparison of gene expression levels between HeLa-Cx46 and HeLa wild-type cells is shown, indicating the fold changes in mRNA levels. This analysis reveals the impact of Cx46 on gene expression and its potential role in modulating transcriptional activity in HeLa cells

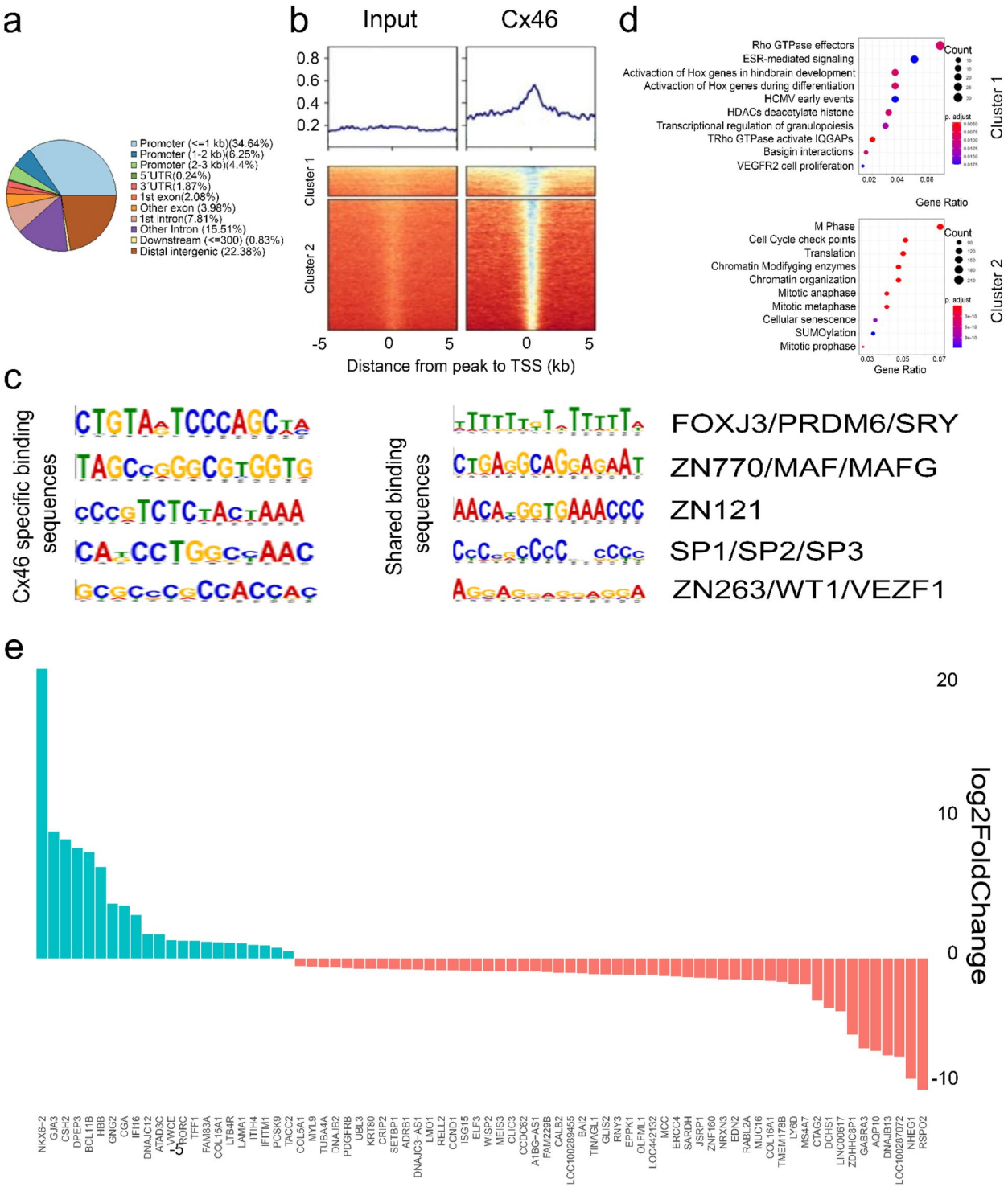

Fig. 4 (See legend on previous page.)

Cx46 may also produce alternatively translated isoforms. Of particular interest was the 30 kDa fragment of Cx46 that was detected by the anti-Cx46 antibody in HeLa cells. To investigate this, we mutated Cx46's methionine residues at positions 102 (M2), 141 (M3), 207 (M4), and 219 (M5) to alanine, one at a time. Western blot analysis of HeLa cells expressing Cx46 revealed several bands, with the most prominent at 30, 46, 53,

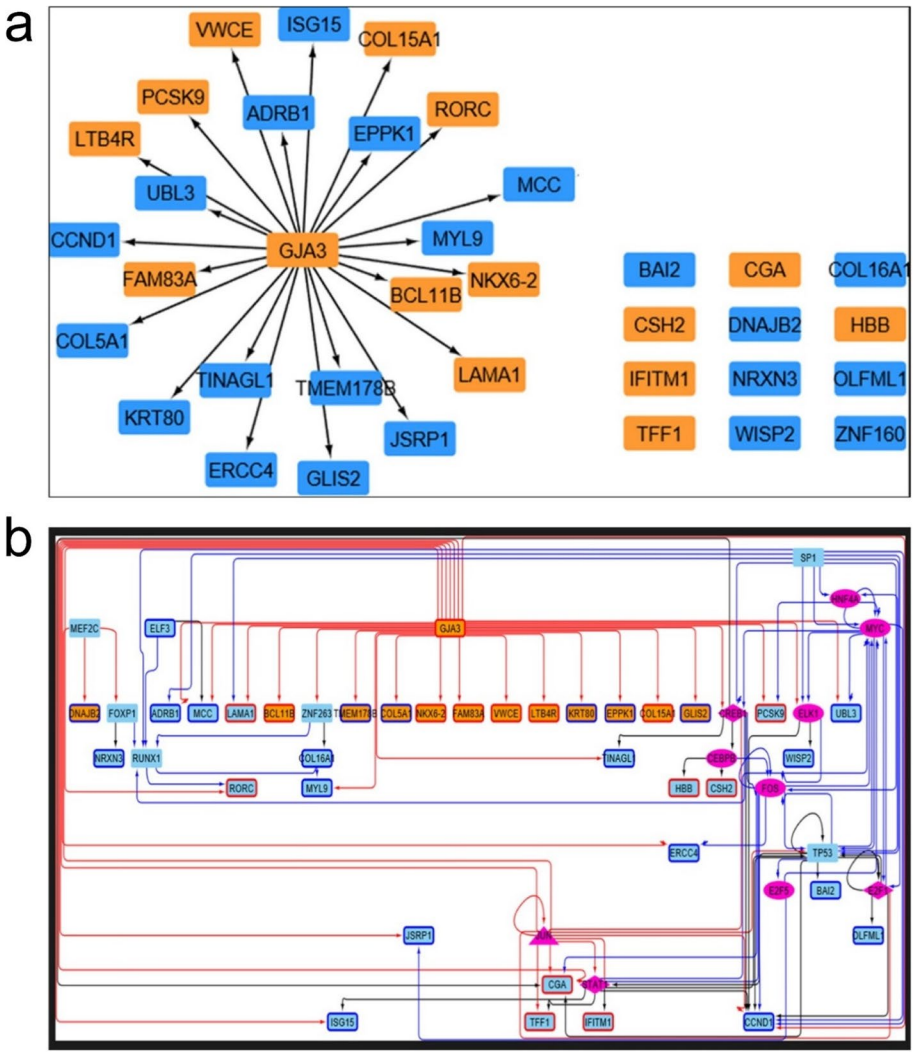

Fig. 5 Association of Cx46 with differential gene expression in HeLa cells. **a** Cx46 association with differentially expressed genes: This panel displays a representation of 23 genes that exhibit altered expression in HeLa-Cx46 cells. Genes with Cx46 enrichment peaks in their promoter regions are indicated by arrows. Up-regulated genes are represented in orange boxes, while down-regulated genes are represented by light blue boxes. Additionally, some genes are differentially expressed but lack direct Cx46 binding at their transcription start site (TSS), indicated by separate boxes with arrows. **b** Cx46-regulated gene network: A network diagram illustrates the regulatory network influenced by Cx46. This network was constructed by integrating data from Chip-seq, RNA-seq, and databases RegNetwork and DoRothEA. Up-regulated genes are depicted in orange boxes, while down-regulated genes are shown by light blue boxes

57, and 68 kDa (Fig. 6b). Interestingly, the M2, M4, and M5 mutants showed similar band patterns, but the M3 mutant lacked the 30 KDa band, indicating that this isoform (GJA3-30 k) arises from alternative translation at Met141. Given that the 68 kDa band has previously been reported to correspond to a phosphorylated form of Cx46 [26, 70], it is likely that the bands with a molecular weight greater than 46 KDa (53 and 57 KDa) also correspond to different phosphorylated forms of Cx46. In consequence, the lack of the 30 KDa isoform could be modulating Cx46 phosphorylation patterns. To determine whether GJA3-30 k interacts with DNA, we generated dimeric models, as many DNA-binding proteins function as dimers [71]. Using Molecular dynamics (MD), we obtained three distinct DNA-GJA-30 k structures, with the main cluster representing over 60% of the total structures. This structure showed consistent stability throughout the 500 ns simulation, evaluated based on the convergence of the Root Mean Square Deviation. We found that residues 141 to 241 may form a 'tweezer' that surrounds DNA (Fig. 6c). Interestingly, structural similarities between RAD50 (PDB ID:

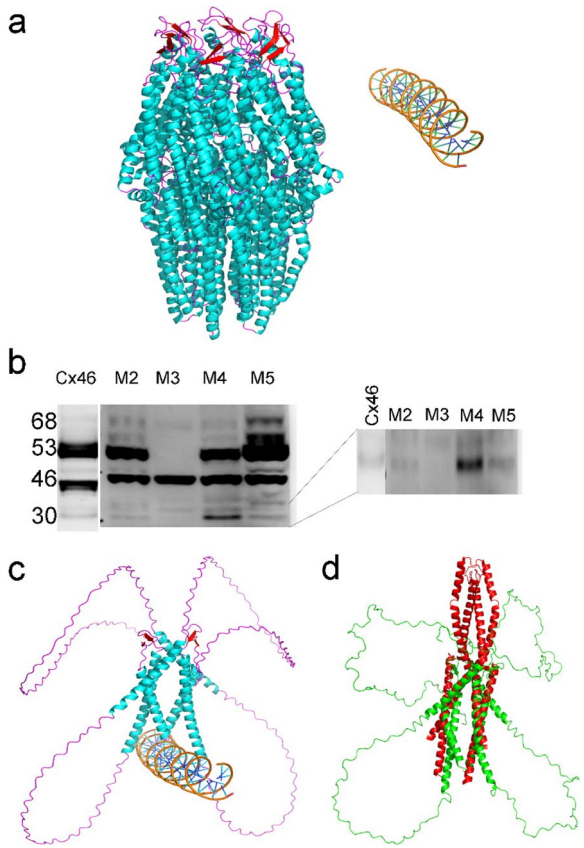

Fig. 6 GJA3-30 k has the potential to interact with DNA. **a** A representative model of the Cx46 hexamer and DNA interactions, as predicted by AlphaFold3, suggesting potential DNA-binding capacity for Cx46. **b** HeLa cells were transfected with wild-type Cx46 or mutants in which the second (M2), third (M3), fourth (M4), and fifth (M5) methionines were replaced with alanine. A zoomed-in Western blot (right panel) reveals that the 30 kDa fragment is absent exclusively in the M3 mutant, suggesting its critical role in the generation of the GJA3-30 k fragment. **c** A structural model of the DNA-bound GJA3-30 k complex, as predicted by AlphaFold3. **d** Superimposed structures of GJA3-30 k (green) and RAD50 (red), illustrating structural similarities between GJA3-30 k and RAD50, a protein essential for DNA repair and cell cycle regulation

5GOX), a protein involved in repairing double-strand DNA breaks which contains a coiled-coil zinc-hook motif designed for DNA binding and GJA3-30 k were found using Dali server (Fig. 6d).

Both Cx46 and the GJA3-30 k isoform are present in the nuclei of prostate, melanoma and breast cancer cell lines

To determine whether Cx46 and/or GJA3-30 k are present in the nuclei of cancer cells beyond HeLa and Sk-Mel-2, we performed nuclear isolation and Western blot analyses in prostate (DU145, LnCap, PC3), melanoma (Sk-Mel-2, Mel-1, 397Mel), and breast (ZR75, MDA-MB-231) cancer cell lines. Laminin B was used as nuclear marker and GAPDH and actin as cytoplasmic markers. As expected, the nuclear marker Laminin B was almost exclusively present in the nuclear fractions (Fig. 7, N lanes), while GAPDH and actin were predominantly cytoplasmic (Fig. 7, C lanes). In prostate, melanoma, and breast cancer cells, Cx46 was detected in both the nuclear and cytoplasmic fractions, and notably, GJA3-30 k was clearly present in the nucleus of melanoma cell lines, however we van not discharge low levels in the other cell lines. These findings reinforce our previous observations and suggest that Cx46 and its alternatively translated isoform GJA3-30 k may act as transcriptional regulators in multiple cancer types.

Discussion

Our findings reveal that Cx46 expression in HeLa cells is associated with mesenchymal and CSC traits, enhancing invasiveness through interactions with cancer-related gene promoters. Confocal immunofluorescence and biochemical analyses confirm its nuclear localization, which is consistent with its co-localization with Nopp-140 in pituitary folliculostellate cells [26]. The detection of a 30 kDa band in nuclear extracts suggests a role in gene regulation, aligning with evidence that Cx C-terminal domains interact with proteins to modulate gene expression, proliferation, and migration [10, 72–76]. Additionally, Cx26 and Cx43 may directly bind nucleotides [77], reinforcing Cx46's involvement in transcriptional regulation. Although Cxs exhibit both anti- and pro-tumorigenic properties [78], Cx46 is predominantly pro-tumorigenic, driving mesenchymal and CSC traits in breast cancer and glioblastoma models [21–24]. While its role in cancer progression is well accepted, underlying mechanisms remain unclear. Beyond their ion channel function, Cxs interact with proteins and DNA. This study provides the first evidence that Cx46 acts as a transcriptional regulator in cancer, upregulating oncogenes and increasing invasiveness. Notably, Cx46 motif analysis identified binding sites for SP1 and ZNF263, both implicated in cancer progression and therapy resistance [79–83]. Their presence in the Cx46 regulatory network suggests they may act as co-regulators, warranting further investigation.

Cx46's role in HeLa cells aligns with findings in glioblastoma and MCF-7 breast cancer cells [21–24], indicating that its function is not cell type-dependent. TCGA data confirmed its upregulation across cancers, but its impact may depend more on its nuclear localization than in its expression levels alone. While elevated in breast invasive carcinoma and linked to aggressive MCF-7 phenotypes [24], a meta-analysis of ~ 1900 breast cancer patients found no correlation between overall Cx46 protein levels and survival [84]. Similarly, Cx43's membrane

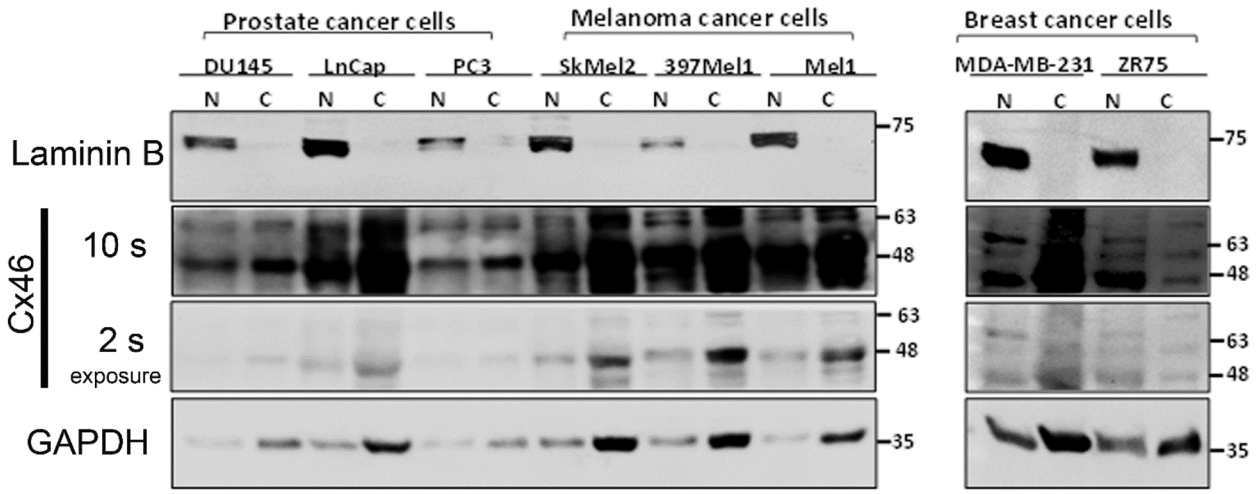

Fig. 7 Western blot analysis of nuclear and cytoplasmic protein fractions from prostate cancer (DU145, LNCaP, and PC3), melanoma (SkMel2, 397Mel, and Mel1), and breast cancer (MDA-MB-231 and ZR75) cell lines. Lamin B1 was used as a nuclear purity control (N) and GAPDH and actin as cytoplasmic markers (C). The western blots demonstrate Cx46 expression across all analyzed cell lines, presented at both high and low exposure times. Cx46 is observed at molecular weights of approximately 68, 63, 46 kDa. Additionally, the melanoma cell lines show the presence of GJA3-30 K. Two exposure times for Cx46 are shown: one at 2 s and the other at 10 s, in order to highlight bands with lower abundance

localization correlates with greater survival, whereas its cytoplasmic localization does not [85]. Our findings suggest that nuclear Cx46 may contribute to a more aggressive phenotype, emphasizing the need to investigate its localization in cancer progression.

Dysregulated TF activity in cancer cells enhances aggressiveness, metastasis, and chemoresistance [86]. Understanding how these TFs drive malignancy is crucial for cancer therapy development [87]. Our gene network analysis reveals that Cx46 modulates TP53 and Myc—genes frequently altered in cancer and linked to poor prognosis [88, 89]. This suggests that Cx46 may amplify oncogene activity and activate malignancy-associated pathways, highlighting its potential as a therapeutic target. A key discovery is that GJA3-30 k localizes in the nucleus, where molecular simulations suggest it interacts with DNA as a dimer. Its 3D structure resembles RAD50, a protein essential for DNA repair and cell cycle regulation. Future analyses could determine whether GJA3-30 k forms structures similar to known TFs, such as zinc finger proteins. Unlike most Cxs, which are ubiquitously expressed throughout the human body, Cx46 is physiologically expressed exclusively in the eye lens [19]. This unique expression pattern makes it a promising candidate for use as a biomarker for tumor invasiveness, as its absence in non-tumoral cells would minimize false positives. Additionally, its potential as a therapeutic target is particularly interesting, as a drug targeting Cx46 could have reduced systemic side effects, with the primary concern being its impact on lens transparency.

In conclusion, this study redefines Cx46 as a transcriptional regulator in cancer. Its ability to upregulate oncogenes and drive invasiveness underscores a novel tumorigenic mechanism. The identification of SP1 and ZNF263 as potential co-regulators adds complexity to its regulatory network. Further research is needed to elucidate the molecular and clinical implications of Cx46 in cancer progression.

Supplementary Information

The online version contains supplementary material available at https://doi.org/10.1186/s12964-025-02151-w.

Supplementary Material 1

Acknowledgements
We would like to thank the doctorate in sciences and innovation in medicine (DICIM) at UDD, for its support in AFO´s PhD thesis. Microscopy facility at Centro Ciencia & Vida, FB210008, Financiamiento Basal para Centros Científicos y Tecnológicos de Excelencia de ANID

Authors' contributions
AFO, AJMM, MAS, MAR designed the study, AFO, VPO, JLL, GN, PPM, SCR, IEA carried out the experiments, MAR, MAS, JFC, FM, JS and MAS wrote and edited the manuscript. AFO, GN, SCR, AJMM, and MAS carried out the computational analysis. All authors have read, commented and approved the manuscript final form.

Funding
Centro Ciencia & Vida, FB210008, Financiamiento Basal para Centros Científicos y Tecnológicos de Excelencia de ANID. FONDECYT Postdoctorado 3220673 (to JSCR). Powered@NLHPC: This research/thesis was partially supported by the supercomputing infrastructure of the NLHPC (ECM-02). This research was partially supported by the FONDEQUIP Grant EQM190110. This research was partially supported by the doctorate in science and innovation in medicine (DICIM) at Universidad del Desarrollo. Proyectos Fondecyt 11171015 (MS), 1240485 (MAR) and 1240804 (JS).

Data availability
All data will be available as requested. We have uploaded CHIPseq and RNAseq raw data in the following link https://drive.google.com/drive/folders/1p-nnnDqkkZeEhEJbYuZJ-LfquAErD3WU?usp=sharing.

Declarations

Ethics approval and consent to participate
Not applicable.

Consent for publication
Not applicable.

Competing interests
The authors declare no competing interests.

Author details
[1]Programa de Comunicación Celular en Cáncer, Instituto de Ciencias e Innovación en Medicina, Facultad de Medicina, Clínica Alemana Universidad del Desarrollo, Santiago, Chile. [2]Plant Genome Regulation Lab, Centro de Biotecnología Vegetal, Facultad de Ciencias de la Vida, Universidad Andrés Bello, Santiago, Chile. [3]Laboratorio de Redes Biológicas, Centro Científico y Tecnológico de Excelencia Ciencia & Vida, Fundación Ciencia & Vida, Santiago, Chile. [4]Escuela de Ingeniería, Facultad de Ingeniería, Arquitectura y Diseño, Universidad San Sebastián, Santiago, Chile. [5]Department of Physics and Astronomy "G. Galilei", University of Padova, Institute of Biochemistry and Cell Biology, Italian National Research Council, 00015 Monterotondo, Padova 35131, Italy. [6]Centro de Genética y Genómica, Instituto de Ciencias e Innovación en Medicina, Facultad de Medicina Clínica Alemana Universidad del Desarrollo, Santiago, Chile. [7]Laboratorio de Neurobiología, Instituto de Ciencias Biomédicas, Facultad de Medicina, Universidad Andres Bello, Santiago 8370146, Chile. [8]Departamento de Procesos Diagnósticos y Evaluación, Laboratorio de Investigación en Salud de Precisión, Facultad de Ciencias de la Salud, Universidad Católica de Temuco, Temuco, Chile. [9]Centro Ciencia & Vida, Fundación Ciencia & Vida. Nuñoa, Santiago, Chile. [10]Translational Medicine Laboratory, Instituto Oncológico Fundación Arturo López Pérez, Santiago 7500691, Chile.

Received: 13 November 2024 Accepted: 11 March 2025
Published online: 27 March 2025

References

1. Sung H, Ferlay J, Siegel RL, Laversanne M, Soerjomataram I, Jemal A, et al. Global Cancer Statistics 2020 : GLOBOCAN Estimates of Incidence and Mortality Worldwide for 36 Cancers in 185 Countries. 2021;71:209–49.
2. Calabrese C, Davidson NR, Demircioglu D, Fonseca NA, He Y, Kahles A, et al. Genomic basis for RNA alterations in cancer. Nat 2020 5787793. Nature Publishing Group; 2020;578:129–36. Available from: https://www.nature.com/articles/s41586-020-1970-0. Cited 2022 Oct 11.
3. Fatima S, Kumar V, Kumar D. Molecular mechanism of genetic, epigenetic, and metabolic alteration in lung cancer. Med Oncol. Med Oncol; 2025;42:61. Available from: https://pubmed.ncbi.nlm.nih.gov/39893601/. Cited 2025 Feb 2.
4. Saez J, Berthoud V, Branes M, Martinez A, Beyer E. Plasma membrane channels formed by connexins: their regulation and functions. Physiol Rev. Physiol Rev; 2003;83:1359–400. Available from: https://pubmed.ncbi.nlm.nih.gov/14506308/. Cited 2021 Jul 27.
5. Phillips SL, Williams CB, Zambrano JN, Williams CJ, Yeh ES. Connexin 43 in the development and progression of breast cancer : What ' s the connection ? (Review). 2017;1005–13.
6. Leithe E, Mesnil M, Aasen T. The connexin 43 C-terminus: A tail of many tales. Biochim Biophys Acta - Biomembr. 2018;1860:48–64. Available from: http://www.ncbi.nlm.nih.gov/pubmed/28526583. Cited 2018 Aug 13.
7. Sorgen P, Trease A, Spagnol G, Delmar M, Nielsen M. Protein-Protein Interactions with Connexin 43: Regulation and Function. Int J Mol Sci. 2018;19:1428.
8. Giepmans BNG, Verlaan I, Moolenaar WH. Connexin-43 interactions with ZO-1 and alpha- and beta-tubulin. Cell Commun Adhes. 2001;8:219–23. Available from: http://www.ncbi.nlm.nih.gov/pubmed/12064592. Cited 2020 Apr 15.
9. Hervé JC, Bourmeyster N, Sarrouilhe D. Diversity in protein-protein interactions of connexins: Emerging roles. Biochim. Biophys. Acta - Biomembr. Biochim Biophys Acta; 2004. p. 22–41.
10. Kotini M, Barriga EH, Leslie J, Gentzel M, Rauschenberger V, Schambony A, et al. Gap junction protein Connexin-43 is a direct transcriptional regulator of N-cadherin in vivo. Nat Commun. 2018;9:3846. Available from: http://www.ncbi.nlm.nih.gov/pubmed/30242148. Cited 2019 Feb 26.
11. Dang X, Doble BW, Kardami E. The carboxy-tail of connexin-43 localizes to the nucleus and inhibits cell growth. Mol Cell Biochem. 2003;242:35–8. Available from: http://www.ncbi.nlm.nih.gov/pubmed/12619863. Cited 2018 Nov 13.
12. Martins-Marques T, Witschas K, Ribeiro I, Zuzarte M, Catarino S, Ribeiro-Rodrigues T, et al. Cx43 can form functional channels at the nuclear envelope and modulate gene expression in cardiac cells. Open Biol. Open Biol; 2023;13. Available from: https://pubmed.ncbi.nlm.nih.gov/37907090/. Cited 2024 Jul 9.
13. Epifantseva I, Xiao S, Baum RE, Kléber AG, Hong T, Shaw RM. An Alternatively Translated Connexin 43 Isoform, GJA1–11k, Localizes to the Nucleus and Can Inhibit Cell Cycle Progression. Biomolecules. MDPI AG; 2020;10:473.
14. Thiagarajan PS, Sinyuk M, Turaga SM, Mulkearns-Hubert EE, Hale JS, Rao V, et al. Cx26 drives self-renewal in triple-negative breast cancer via interaction with NANOG and focal adhesion kinase. Nat Commun Nature Publishing Group. 2018;9:1–14.
15. Mulkearns-Hubert EE, Rhoades EE, Ben-Salem S, Bharti R, Hajdari N, Johnson S, et al. Targeting NANOG and FAK via Cx26-derived Cell-penetrating Peptides in Triple-negative Breast Cancer. Mol Cancer Ther. Mol Cancer Ther; 2024;23:56–67. Available from: https://pubmed.ncbi.nlm.nih.gov/37703580/. Cited 2024 Jul 9.
16. Lillo MA, Muñoz M, Rhana P, Gaul-Muller K, Quan J, Shirokova N, et al. Remodeled connexin 43 hemichannels alter cardiac excitability and promote arrhythmias. J Gen Physiol. J Gen Physiol; 2023 [cited 2023 Jul 6];155. Available from: https://pubmed.ncbi.nlm.nih.gov/37191672/
17. Stehberg J, Moraga-Amaro R, Salazar C, Becerra A, Echeverría C, Orellana JA, et al. Release of gliotransmitters through astroglial connexin 43 hemichannels is necessary for fear memory consolidation in the basolateral amygdala. FASEB J. 2012;26(9):3649–57. https://doi.org/10.1096/fj.11-198416.
18. Kojima T, Mitaka T, Shibata Y, Mochizuki Y. Induction and regulation of connexin26 by glucagon in primary cultures of adult rat hepatocytes. J Cell Sci. J Cell Sci; 1995;108 (Pt 8):2771–80. Available from: https://pubmed.ncbi.nlm.nih.gov/7593318/. Cited 2024 Jul 9.
19. Retamal MA, Altenberg GA. Role and Posttranslational Regulation of Cx46 Hemichannels and Gap Junction Channels in the Eye Lens. Front Physiol. Front Physiol; 2022;13. Available from: https://pubmed.ncbi.nlm.nih.gov/35431975/. Cited 2022 Jul 19.
20. Banerjee D, Gakhar G, Madgwick D, Hurt A, Takemoto D, Nguyen TA. A novel role of gap junction connexin46 protein to protect breast tumors from hypoxia. Int J cancer NIH Public Access. 2010;127:839–48.
21. Hitomi M, Deleyrolle LP, Mulkearns-Hubert EE, Jarrar A, Li M, Sinyuk M, et al. Differential Connexin Function Enhances Self-Renewal in Glioblastoma. Cell Rep. Elsevier; 2015;11:1031–42. Available from: http://www.ncbi.nlm.nih.gov/pubmed/25959821. Cited 2020 Apr 18.
22. Banerjee D. Connexin's connection in breast cancer growth and progression. Int J Cell Biol. Hindawi Publishing Corporation; 2016;2016.
23. Burr DB, Molina SA, Banerjee D, Low DM, Takemoto DJ. Treatment with connexin 46 siRNA suppresses the growth of human Y79 retinoblastoma cell xenografts in vivo. Exp Eye Res. 2011;92:251–9. Available from: http://www.ncbi.nlm.nih.gov/pubmed/21320488. Cited 2018 Nov 20.
24. Acuña RA, Varas-Godoy M, Herrera-Sepulveda D, Retamal MA. Connexin46 Expression Enhances Cancer Stem Cell and Epithelial-to-Mesenchymal Transition Characteristics of Human Breast Cancer MCF-7 Cells. Int J Mol Sci. Int J Mol Sci; 2021;22. Available from: https://pubmed.ncbi.nlm.nih.gov/34830485/. Cited 2022 May 26.
25. León-Fuentes IM, Salgado-Gil MG, Novoa MS, Retamal MA. Connexins in Cancer, the Possible Role of Connexin46 as a Cancer Stem Cell-Determining Protein. Biomolecules. Biomolecules; 2023 [cited 2024 Jun 26];13. Available from: https://pubmed.ncbi.nlm.nih.gov/37892142/

26. Vitale ML, Garcia CJ, Akpovi CD, Pelletier R-M. Distinctive actions of connexin 46 and connexin 50 in anterior pituitary folliculostellate cells. Tabernero A, editor. PLoS One. 2017;12:e0182495. Available from: https://dx.plos.org/https://doi.org/10.1371/journal.pone.0182495. Cited 2018 Nov 13.
27. Hacot S, Coute Y, Alexandra M, Mertani HC, Sanchez J, Diaz J. Isolation of Nucleoli. 2010;1–10.Hacot S, Coute Y, Belin S, Albaret MA, Mertani HC, Sanchez JC, Rosa-Calatrava M, Diaz JJ. Isolation of nucleoli. Curr Protoc Cell Biol. 2010;Chapter 3:Unit3.36. https://doi.org/10.1002/0471143030.cb0336s47.
28. Justus CR, Marie MA, Sanderlin EJ, Yang L V. Transwell In Vitro Cell Migration and Invasion Assays. Methods Mol Biol. Methods Mol Biol; 2023;2644:349–59. Available from: https://pubmed.ncbi.nlm.nih.gov/37142933/. Cited 2024 Jul 11.
29. Pérez-Moreno P, Riquelme I, Bizama C, Vergara-Gómez L, Tapia JC, Brebi P, et al. LINC00662 Promotes Aggressive Traits by Modulating OCT4 Expression through miR-335–5p in Gallbladder Cancer Cells. Int J Mol Sci. Int J Mol Sci; 2024;25. Available from: https://pubmed.ncbi.nlm.nih.gov/38928444/. Cited 2025 Jan 31.
30. Lachmann A, Torre D, Keenan AB, Jagodnik KM, Lee HJ, Wang L, et al. Massive mining of publicly available RNA-seq data from human and mouse. Nat Commun. Nat Commun; 2018;9. Available from: https://pubmed.ncbi.nlm.nih.gov/29636450/. Cited 2022 Oct 11.
31. Love MI, Huber W, Anders S. Moderated estimation of fold change and dispersion for RNA-seq data with DESeq2. Genome Biol. Genome Biol; 2014;15. Available from: https://pubmed.ncbi.nlm.nih.gov/25516281/. Cited 2022 Oct 11.
32. Fernandez-Olivares A, Retamal MA. Protocol for the Study of Connexin and DNA Interactions. Methods Mol Biol. Methods Mol Biol; 2024;2801:125–34. Available from: https://pubmed.ncbi.nlm.nih.gov/38578418/. Cited 2024 Jun 29.
33. Ren X, Shao Y, Zhang Y, Ni Y, Bi Y, Li R. Primerdiffer: a python command-line module for large-scale primer design in haplotype genotyping. Bioinformatics. Bioinformatics; 2023;39. Available from: https://pubmed.ncbi.nlm.nih.gov/37067484/. Cited 2023 May 18.
34. Heinz S, Benner C, Spann N, Bertolino E, Lin YC, Laslo P, et al. Simple combinations of lineage-determining transcription factors prime cis-regulatory elements required for macrophage and B cell identities. Mol Cell. Mol Cell; 2010;38:576–89. Available from: https://pubmed.ncbi.nlm.nih.gov/20513432/. Cited 2022 Oct 11.
35. Yu G, Wang LG, He QY. ChIPseeker: an R/Bioconductor package for ChIP peak annotation, comparison and visualization. Bioinformatics. Bioinformatics; 2015;31:2382–3. Available from: https://pubmed.ncbi.nlm.nih.gov/25765347/. Cited 2022 Oct 11.
36. Bailey TL. Discovering Novel Sequence Motifs with MEME. Curr Protoc Bioinforma. Wiley; 2003;00. 2.4.1-2.4.35. https://doi.org/10.1002/0471250953.bi0204s00.
37. Santander N, Lizama C, Murgas L, Contreras S, Martin AJM, Molina P, et al. Transcriptional profiling of embryos lacking the lipoprotein receptor SR-B1 reveals a regulatory circuit governing a neurodevelopmental or metabolic decision during neural tube closure. BMC Genomics. BMC Genomics; 2018;19. Available from: https://pubmed.ncbi.nlm.nih.gov/30290792/. Cited 2023 Mar 24.
38. Murgas L, Contreras-Riquelme S, Martínez-Hernandez JE, Villaman C, Santibáñez R, Martin AJM. Automated generation of context-specific gene regulatory networks with a weighted approach in Drosophila melanogaster. Interface Focus. Interface Focus; 2021 [cited 2023 Mar 24];11. Available from: https://pubmed.ncbi.nlm.nih.gov/34123358/
39. Han H, Cho JW, Lee S, Yun A, Kim H, Bae D, et al. TRRUST v2: an expanded reference database of human and mouse transcriptional regulatory interactions. Nucleic Acids Res. Nucleic Acids Res; 2018;46:D380–6. Available from: https://pubmed.ncbi.nlm.nih.gov/29087512/. Cited 2023 Mar 24.
40. Liu ZP, Wu C, Miao H, Wu H. RegNetwork: an integrated database of transcriptional and post-transcriptional regulatory networks in human and mouse. Database (Oxford). Database (Oxford); 2015;2015:1–12. Available from: https://pubmed.ncbi.nlm.nih.gov/26424082/. Cited 2023 Mar 24.
41. Garcia-Alonso L, Holland CH, Ibrahim MM, Turei D, Saez-Rodriguez J. Benchmark and integration of resources for the estimation of human transcription factor activities. Genome Res. Genome Res; 2019;29:1363–75. Available from: https://pubmed.ncbi.nlm.nih.gov/31340985/. Cited 2023 Mar 24.
42. Holland CH, Szalai B, Saez-Rodriguez J. Transfer of regulatory knowledge from human to mouse for functional genomics analysis. Biochim Biophys acta Gene Regul Mech. Biochim Biophys Acta Gene Regul Mech; 2020;1863. Available from: https://pubmed.ncbi.nlm.nih.gov/31525460/. Cited 2023 Mar 24.
43. Zerbino DR, Wilder SP, Johnson N, Juettemann T, Flicek PR. The ensembl regulatory build. Genome Biol. Genome Biol; 2015;16. Available from: https://pubmed.ncbi.nlm.nih.gov/25887522/. Cited 2023 May 19.
44. Davis TL, Rebay I. Master regulators in development: Views from the Drosophila retinal determination and mammalian pluripotency gene networks. Dev Biol. Dev Biol; 2017;421:93–107. Available from: https://pubmed.ncbi.nlm.nih.gov/27979656/. Cited 2023 Mar 24.
45. Szklarczyk D, Gable AL, Lyon D, Junge A, Wyder S, Huerta-Cepas J, et al. STRING v11: protein-protein association networks with increased coverage, supporting functional discovery in genome-wide experimental datasets. Nucleic Acids Res. Nucleic Acids Res; 2019;47:D607–13. Available from: https://pubmed.ncbi.nlm.nih.gov/30476243/. Cited 2023 Mar 24.
46. Abramson J, Adler J, Dunger J, Evans R, Green T, Pritzel A, et al. Accurate structure prediction of biomolecular interactions with AlphaFold 3. Nat 2024 6308016. Nature Publishing Group; 2024;630:493–500. Available from: https://www.nature.com/articles/s41586-024-07487-w. Cited 2024 Oct 9.
47. Abraham MJ, Murtola T, Schulz R, Páll S, Smith JC, Hess B, et al. GROMACS: High performance molecular simulations through multi-level parallelism from laptops to supercomputers. SoftwareX Elsevier. 2015;1–2:19–25.
48. Jo S, Kim T, Iyer VG, Im W. CHARMM-GUI: a web-based graphical user interface for CHARMM. J Comput Chem. J Comput Chem; 2008;29:1859–65. Available from: https://pubmed.ncbi.nlm.nih.gov/18351591/. Cited 2024 Oct 9.
49. Gowers R, Linke M, Barnoud J, Reddy T, Melo M, Seyler S, et al. MDAnalysis: A Python Package for the Rapid Analysis of Molecular Dynamics Simulations. Proc 15th Python Sci Conf. SciPy; 2016;98–105. Available from: https://proceedings.scipy.org/articles/Majora-629e541a-00e. Cited 2024 Oct 9.
50. Holm L. Dali server: structural unification of protein families. Nucleic Acids Res. Nucleic Acids Res; 2022;50:W210–5. Available from: https://pubmed.ncbi.nlm.nih.gov/35610055/. Cited 2024 Oct 9.
51. Liu J, Lichtenberg T, Hoadley KA, Poisson LM, Lazar AJ, Cherniack AD, et al. An Integrated TCGA Pan-Cancer Clinical Data Resource to Drive High-Quality Survival Outcome Analytics. Cell. Cell Press; 2018;173:400. Available from: https://pmc.ncbi.nlm.nih.gov/articles/PMC6066282/. Cited 2024 Nov 12.
52. Fernández-Olivarez Ainoa, Duran Eduardo , Verdugo Daniel A. , Fiori Mariana C, Altenberg Guillermo A, Stehberg Jimmy, Alfaro Iván, Calderón Juan Francisco RMA. Extracellular cysteines are critical to form functional Cx46 hemichannels. Int J Mol Sci. 2022.
53. Jinesh GG, Brohl AS. Classical epithelial-mesenchymal transition (EMT) and alternative cell death process-driven blebbishield metastatic-witch (BMW) pathways to cancer metastasis. Signal Transduct Target Ther. Signal Transduct Target Ther; 2022;7:296. Available from: https://pubmed.ncbi.nlm.nih.gov/35999218/. Cited 2022 Oct 11.
54. Guo X, Chen Y, Ji W, Chen X, Li C, Ge R. Enrichment of cancer stem cells by agarose multi-well dishes and 3D spheroid culture. Cell Tissue Res. Cell Tissue Res; 2019;375:397–408. Available from: https://pubmed.ncbi.nlm.nih.gov/30244317/. Cited 2023 Dec 22.
55. Thomson SP, Meyskens FL. Method for Measurement of Self-Renewal Capacity of Clonogenic Cells from Biopsies of Metastatic Human Malignant Melanoma. Cancer Res. 1982;42:4606–13.
56. Ishiguro T, Ohata H, Sato A, Yamawaki K, Enomoto T, Okamoto K. Tumor-derived spheroids: Relevance to cancer stem cells and clinical applications. Cancer Sci. Wiley-Blackwell; 2017;108:283. Available from: /pmc/articles/PMC5378268/. Cited 2023 Dec 22.
57. O'Brien CA, Kreso A, Jamieson CHM. Cancer stem cells and self-renewal. Clin. Cancer Res. Clin Cancer Res. 2010;16(12):3113–20. https://doi.org/10.1158/1078-0432.CCR-09-2824.
58. Abbaszadegan MR, Bagheri V, Razavi MS, Momtazi AA, Sahebkar A, Gholamin M. Isolation, identification, and characterization of cancer stem cells: A review. J Cell Physiol. 2017;232(8):2008–18. https://doi.org/10.1002/jcp.25759.
59. Wang SS, Jiang J, Liang XH, Tang YL. Links between cancer stem cells and epithelial-mesenchymal transition. Onco Targets Ther. Onco Targets Ther;

2015;8:2973–80. Available from: https://pubmed.ncbi.nlm.nih.gov/26527883/. Cited 2022 Oct 11.
60. Lv T, Wang C, Zhou J, Feng X, Zhang L, Fan Z. Mechanism and role of nuclear laminin B1 in cell senescence and malignant tumors. Cell death Discov. Cell Death Discov; 2024;10. Available from: https://pubmed.ncbi.nlm.nih.gov/38824174/. Cited 2025 Feb 3.
61. Visa N, Percipalle P. Nuclear functions of actin. Cold Spring Harb Perspect Biol. Cold Spring Harb Perspect Biol; 2010;2. Available from: https://pubmed.ncbi.nlm.nih.gov/20452941/. Cited 2025 Feb 3.
62. Yi J, Ren L, Li D, Wu J, Li W, Du G, et al. Trefoil factor 1 (TFF1) is a potential prognostic biomarker with functional significance in breast cancers. Biomed Pharmacother. Biomed Pharmacother; 2020;124. Available from: https://pubmed.ncbi.nlm.nih.gov/31986408/. Cited 2022 Oct 11.
63. Yan J, Jiang Y, Lu J, Wu J, Zhang M. Inhibiting of Proliferation, Migration, and Invasion in Lung Cancer Induced by Silencing Interferon-Induced Transmembrane Protein 1 (IFITM1). Biomed Res Int. Biomed Res Int; 2019;2019. Available from: https://pubmed.ncbi.nlm.nih.gov/31205947/. Cited 2022 Oct 11.
64. Sakamoto S, Inoue H, Kohda Y, Ohba SI, Mizutani T, Kawada M. Interferon-Induced Transmembrane Protein 1 (IFITM1) Promotes Distant Metastasis of Small Cell Lung Cancer. Int J Mol Sci. Int J Mol Sci; 2020;21:1–17. Available from: https://pubmed.ncbi.nlm.nih.gov/32668617/. Cited 2022 Oct 11.
65. Chen S, Huang J, Liu Z, Liang Q, Zhang N, Jin Y. FAM83A is amplified and promotes cancer stem cell-like traits and chemoresistance in pancreatic cancer. Oncogenesis. Oncogenesis; 2017;6. Available from: https://pubmed.ncbi.nlm.nih.gov/28287611/.Cited 2023 May 18.
66. Schiavi A, Hudder A, Werner R. Connexin43 mRNA contains a functional internal ribosome entry site. FEBS Lett. 1999;464(3):1183–22. https://doi.org/10.1016/s0014-5793(99)01699-3.
67. Salat-Canela C, Sesé M, Peula C, Ramón Y Cajal S, Aasen T. Internal translation of the connexin 43 transcript. Cell Commun Signal. Signal Transduction Society; 2014;12:31. Available from: http://www.ncbi.nlm.nih.gov/pubmed/24884945. Cited 2020 Apr 15.
68. Ul-Hussain M, Dermietzel R, Zoidl G. Connexins and Cap-independent translation: Role of internal ribosome entry sites. Brain Res. 2012;1487:99–106. https://doi.org/10.1016/j.brainres.2012.05.065.
69. Cai S, Peng F, Tang H, Zhou L, Chen Z, Wu P, et al. A new IRES-mediated truncated Cx32 isoform inhibits global mRNA translation to suppress glioblastoma. Biomed Pharmacother. Biomed Pharmacother; 2023;161. Available from: https://pubmed.ncbi.nlm.nih.gov/36931032/. Cited 2024 Aug 14.
70. Pelletier RM, Akpovi CD, Chen L, Vitale ML. Cholesterol metabolism and Cx43, Cx46, and Cx50 gap junction protein expression and localization in normal and diabetic and obese ob/ob and db/db mouse testes. Am J Physiol Endocrinol Metab. Am J Physiol Endocrinol Metab; 2018;314:E21–38. Available from: https://pubmed.ncbi.nlm.nih.gov/28851737/. Cited 2024 Oct 9.
71. Amoutzias GD, Robertson DL, Van de Peer Y, Oliver SG. Choose your partners: dimerization in eukaryotic transcription factors. Trends Biochem Sci. Trends Biochem Sci; 2008;33:220–9. Available from: https://pubmed.ncbi.nlm.nih.gov/18406148/. Cited 2024 Nov 12.
72. Basheer W, Shaw R. The "tail" of Connexin43: An unexpected journey from alternative translation to trafficking. Biochim. Biophys. Acta - Mol. Cell Res. Elsevier; 2016:1848–56. Available from: http://www.ncbi.nlm.nih.gov/pubmed/26526689. Cited 2020 Apr 15.
73. Dang X, Doble BW, Kardami E. The carboxy-tail of connexin-43 localizes to the nucleus and inhibits cell growth. Mol Cell Biochem. 2003;242:35–8.
74. Kameritsch P, Pogoda K, Pohl U. Channel-independent influence of connexin 43 on cell migration. Biochim Biophys Acta - Biomembr. 2012;1818:1993–2001. Available from: http://www.ncbi.nlm.nih.gov/pubmed/22155212.Cited 2018 Nov 13.
75. Vinken M, Decrock E, Leybaert L, Bultynck G, Himpens B, Vanhaecke T, et al. Biochimica et Biophysica Acta Non-channel functions of connexins in cell growth and cell death ☆. BBA - Biomembr. Elsevier B.V.; 2012;1818:2002–8.
76. Wu J-I, Wang L-H. Emerging roles of gap junction proteins connexins in cancer metastasis, chemoresistance and clinical application. J Biomed Sci. 2019;26:8. Available from: https://jbiomedsci.biomedcentral.com/articles/https://doi.org/10.1186/s12929-019-0497-x. Cited 2019 Jan 18.
77. Varela-Eirin M, Varela-Vazquez A, Rodríguez-Candela Mateos M, Vila-Sanjurjo A, Fonseca E, Mascareñas JL, et al. Recruitment of RNA molecules by connexin RNA-binding motifs: Implication in RNA and DNA transport through microvesicles and exosomes. Biochim Biophys Acta - Mol Cell Res. 2017;1864:728–36. Available from: http://www.ncbi.nlm.nih.gov/pubmed/28167212. Cited 2018 Mar 22.
78. Mulkearns-Hubert EE, Reizes O, Lathia JD. Connexins in Cancer: Jekyll or Hyde? Biomolecules. Multidisciplinary Digital Publishing Institute (MDPI); 2020;10:1–30. Available from: /pmc/articles/PMC7764653/. Cited 2022 Jun 13.
79. Yu Z, Feng J, Wang W, Deng Z, Zhang Y, Xiao L, et al. The EGFR-ZNF263 signaling axis silences SIX3 in glioblastoma epigenetically. Oncogene. Oncogene; 2020;39:3163–78. Available from: https://pubmed.ncbi.nlm.nih.gov/32051553/. Cited 2023 Jan 25.
80. Cui J, Liu J, Fan L, Zhu Y, Zhou B, Wang Y, et al. A zinc finger family protein, ZNF263, promotes hepatocellular carcinoma resistance to apoptosis via activation of ER stress-dependent autophagy. Transl Oncol. Transl Oncol; 2020;13. Available from: https://pubmed.ncbi.nlm.nih.gov/32898766/. Cited 2023 Jan 25.
81. Qian S, Fang H, Zheng L, Liu M. Zingerone suppresses cell proliferation via inducing cellular apoptosis and inhibition of the PI3K/AKT/mTOR signaling pathway in human prostate cancer PC-3 cells. J Biochem Mol Toxicol. John Wiley and Sons Inc; 2021;35. Available from: https://pubmed.ncbi.nlm.nih.gov/32905641/. Cited 2021 Jun 14.
82. Vizcaíno C, Mansilla S, Portugal J. Sp1 transcription factor: A long-standing target in cancer chemotherapy. Pharmacol Ther. Pharmacol Ther; 2015;152:111–24. Available from: https://pubmed.ncbi.nlm.nih.gov/25960131/. Cited 2023 Jan 25.
83. Fan Y, Yang L, Ren Y, Wu Y, Li L, Li L. Sp1-Induced SETDB1 Overexpression Transcriptionally Inhibits HPGD in a β-Catenin-Dependent Manner and Promotes the Proliferation and Metastasis of Gastric Cancer. J Gastric Cancer. J Gastric Cancer; 2022;22:319–38. Available from: https://pubmed.ncbi.nlm.nih.gov/36316108/. Cited 2023 Jan 25
84. Teleki I, Szasz AM, Maros ME, Gyorffy B, Kulka J, Meggyeshazi N, et al. Correlations of Differentially Expressed Gap Junction Connexins Cx26, Cx30, Cx32, Cx43 and Cx46 with Breast Cancer Progression and Prognosis. Scemes E, editor. PLoS One. 2014;9:e112541. Available from: http://www.ncbi.nlm.nih.gov/pubmed/25383624. Cited 2018 May 4.
85. Brockmeyer P, Jung K, Perske C, Schliephake H, Hemmerlein B. Membrane connexin 43 acts as an independent prognostic marker in oral squamous cell carcinoma. Int J Oncol. Int J Oncol. 2014;45:273–81. Available from: https://pubmed.ncbi.nlm.nih.gov/24788723/. Cited 2023 May 19.
86. Lee TI, Young RA. Transcriptional regulation and its misregulation in disease. Cell. Cell; 2013;152:1237–51. Available from: https://pubmed.ncbi.nlm.nih.gov/23498934/. Cited 2022 Oct 12.
87. Bhagwat AS, Vakoc CR. Targeting Transcription Factors in Cancer. Trends in cancer. NIH Public Access; 2015;1:53. Available from: /pmc/articles/PMC4669894/. Cited 2022 Oct 11.
88. Moon JH, Ishii H, Dewi DL, Kano Y, Yamamoto K, Nishikawa S, et al. Gain-of-function oncogenic mutations in TP53 enhance defined factor-mediated cellular reprogramming. Nat Preced 2011. Nature Publishing Group; 2011;1–1. Available from: https://www.nature.com/articles/npre.2011.5681.1. Cited 2022 Oct 12.
89. Sullivan DK, Deutzmann A, Yarbrough J, Krishnan MS, Gouw AM, Bellovin DI, et al. MYC oncogene elicits tumorigenesis associated with embryonic, ribosomal biogenesis, and tissue-lineage dedifferentiation gene expression changes. Oncogene 2022. Nature Publishing Group; 2022;1–11. Available from: https://www.nature.com/articles/s41388-022-02458-9. Cited 2022 Oct 12.

Publisher's Note

Springer Nature remains neutral with regard to jurisdictional claims in published maps and institutional affiliations.